




## Review article

Development of Trastuzumab-coupled, siRNA encapsulating mPolyplexes targeting HER2 overexpressing cancer cells<sup>☆</sup>

Joschka T. Müller<sup>a</sup>, Salvatore Caruso<sup>a,b</sup>, Anny Nguyen<sup>a</sup>, David C. Jürgens<sup>a</sup>,  
Adrian P.E. Kromer<sup>a</sup>, Sahana Sheshachala<sup>c</sup>, Nathan B.P. Adams<sup>c</sup>, Olivia M. Merkel<sup>a,d,e,\*</sup> 

<sup>a</sup> Department of Pharmacy, Ludwig-Maximilians-University Munich, Butenandtstrasse 5-13, Haus B, 81377 Munich, Germany

<sup>b</sup> Department of Pharmacy and Biotechnology, Alma Mater Studiorum, University of Bologna, Via San Donato 19/2, 40127 Bologna, Italy

<sup>c</sup> NanoTemper Technologies GmbH, Steinerstraße 11, Munich 81379, Germany

<sup>d</sup> Center for NanoScience (CeNS), Ludwig-Maximilians-University Munich 80799 Munich, Germany

<sup>e</sup> Ludwig-Maximilians-University Munich, Member of the German Center for Lung Research (DZL), Germany

## ARTICLE INFO

## Keywords:

Ovarian cancer

PBAE

Trastuzumab

siRNA

Polyplexes

Design of experiment

## ABSTRACT

Over the past decades, significant advancements have been made in various medical fields; however, ovarian cancer (OC) remains inadequately addressed, predominantly relying on relatively toxic cytostatic treatments. In this study, we applied newly developed poly( $\beta$ -amino) esters (PBAEs) for siRNA delivery. As recent literature has shown, the introduction of a hydrophobic, unsaturated fatty acid together with polycationic spermines as the PBAE side chains are leading to a favourable transfection efficiency, and the resulting materials form a unique class of micelleplexes, termed micelle-embedded polyplexes (mPolyplexes). Here, such mPolyplexes were modified post-particle formation with the approved monoclonal antibody Trastuzumab for HER2 targeting, as supported by a receptor binding analysis through fluorescence shift assay. Physicochemical analysis revealed suitable hydrodynamic diameters of modified mPolyplexes, as determined by dynamic light scattering. Improved cellular uptake when targeted with Trastuzumab was optimized by applying Design of Experiment (DoE). We demonstrated superior gene silencing efficiency of EGFR as well as PLK1, both involved in OC progression, with knockdown values exceeding 82% and 70%, respectively. These findings were corroborated by a relevant cell migration assay. The macroscopic impact after PLK1 silencing on epithelial-mesenchymal transition (EMT) was visualized using confocal microscopy. This work addresses critical questions in the field of ovarian cancer therapy and confirms the suitability of siRNA encapsulating PBAE nanocarriers as promising non-viral vectors.

## 1. Introduction

Ovarian cancer (OC) is, among other serious diseases for women ranked as the fifth leading cause of death from malignant tumors, with a total mortality exceeding 200,000 cases per year as of 2020 [1] and significant impact on women all across the globe. The high lethality is primarily attributed to poor diagnosis due to misinterpretation of non-specific symptoms [2,3]. Interestingly in OC, prognosis strongly correlates with the timepoint of diagnosis: while there is a 90 % five-year median survival rate in stage I, it drops drastically to only 25 % in a metastatic state [2]. Current treatments for OC, besides surgery, include cytostatic drugs such as taxanes (Paclitaxel and Docetaxel) combined with cis- or carboplatin, intravenously administered anti-VEGF

monoclonal antibody (mAb) bevacizumab, or PARP inhibitors (e.g., Olaparib).

These pharmacological treatments are often limited in specificity, therefore causing severe side effects. In contrast, the use of oligonucleotides like small interfering RNA (siRNA) offers potential benefits in reducing these side effects and could lead to more adherent and safer therapy. An siRNA consists of two complementary RNA strands, each ranging from 21 to 23 nucleotides. Often, siRNAs are chemically modified for a prolonged nuclease stability, resulting in a prolonged half-life, and reduced immunogenicity [4–7]. They exert their pharmacological effect through a mechanism called RNA interference (RNAi). In RNAi, cytosolic siRNA is loaded into the RNA-induced silencing complex (RISC), which is ultimately responsible for mRNA degradation [7]. By

<sup>☆</sup> This article is part of a special issue entitled: 'Bio Mat Interface and Drug Delivery' published in European Journal of Pharmaceutics and Biopharmaceutics.

\* Corresponding author at: Department of Pharmacy, Ludwig-Maximilians-University Munich, Butenandtstrasse 5-13, Haus B, 81377 Munich, Germany.

E-mail address: [olivia.merkel@lmu.de](mailto:olivia.merkel@lmu.de) (O.M. Merkel).

selecting base-complementary RNA sequences, specific mRNA molecules can be silenced, leading to lowered protein expression. Notably, OC is in principle a suitable disease for therapies through RNAi as many different genes were identified to be involved in its emergence. Additionally, localized drug therapy could be possible in the early stages of disease progression [8].

However, due to the highly negative charge of siRNA molecules, they cannot passively diffuse through lipophilic cell membranes, necessitating a suitable delivery system. One group of non-viral drug delivery systems, also called vectors, are poly( $\beta$ -amino) esters (PBAEs). Initially described by Lynn and Langer in 2000 [8], various interpretations of these vectors have been developed over the past more than 20 years [9–13]. PBAEs are economical, scalable, and easy to synthesize in a one-pot Michael addition. A wide range of structures has been investigated, elaborating on the functions of key characteristics such as hydrophilic/lipophilic balance, acidity, molecular weight, branching types, and end-capping. These types of modifications allow researchers to balance the carrier system's properties and develop nanoparticles with distinct, measurable features. An ideal siRNA carrier system would meet several requirements: i) high drug encapsulation, expressed as a full siRNA encapsulation at relatively low polymer excess, ii) low toxicity through the use of biodegradable building blocks, iii) high transfection efficiency, necessitating only small doses of the active pharmaceutical ingredient (API), and iv) a certain specificity for only cells or tissues that need to be treated.

Our group has recently developed and reported PBAEs with alternating substructures consisting out of spermine and oleylamine (OA) moieties to achieve an optimal hydrophilic/lipophilic balance [10,14]. These PBAE are thought to encapsulate negatively charged siRNA through electrostatic interactions, forming polyplexes, or, as hypothesized in a recent study by our group, micelle-embedded Polyplexes (mPolyplexes) [15]. By doing so, we achieved i) full encapsulation at N/P ratios of 5 (up to 30 % (w/w) ratio); ii) the introduction of spermine, a body-own polycation, which encapsulates siRNA using a PBAE biodegradable backbone; iii) transfection efficiencies surpassing polyethyleneimine with moderate toxicity [14], and iv) the potential to incorporate targeting ligands on the primary amine of spermine, which will be explored here.

It was shown that more than 25 % of newly diagnosed OCs show overexpression of human epidermal growth factor receptor 2 (HER2) [16]. To further optimize our PBAE mPolyplexes, we aimed to introduce Trastuzumab as targeting ligand, recently celebrating its 25th year anniversary after FDA approval in 1998 [17]. Originally introduced for the therapy of p185<sup>HER2</sup> overexpressing breast cancer, its development marked a milestone in pharmaceutical development as it was the first approved mAb for the therapy of solid tumors. Nowadays, early-detected HER2-positive breast cancer patients have a median survival rate exceeding 90 % [17], verifying its success history. The interaction of Trastuzumab (Herceptin®) with HER2 on extracellular domain IV prevents ligand-induced dimerization and subsequently downstream signals, which promote cancer formation or metastasis [18]. Notably, in this study, the downstream cancer-preventing effects of Trastuzumab, though significant, were not the primary focus. Instead, Trastuzumab's HER2 targeting effect was used to bring PBAE-nanoparticles into proximity of HER2 overexpressing ovarian cancer cells, facilitating receptor-mediated endocytosis.

Benefitting from active drug targeting, cancer therapeutics aim for a better benefit-risk ratio by targeting cells overexpressing certain characteristics such as receptor status. Non-targeted nanocarriers, in contrast, achieve targeting only passively through the enhanced permeability and retention (EPR) effect [19]. Antibody-drug conjugates, clinically applied as cancer therapies, are the prime example of actively targeted therapies. Other well-known strategies include the introduction of smaller moieties, such as the RGD motifs or folic acid [20–23], in contrast to mAbs, which have high molecular weights (~145,000 Da for Trastuzumab [24]). For attachment, researchers can rely on a wide

range of bioconjugation strategies [25,26] depending on their needs. Here, we used the well-established post-particle formation conjugation strategy, as also recently published by our group with lipid nanoparticles (LNPs) [27]. Using strain-promoted azide-alkyne conjugation (SPAAC), we leveraged easy, highly adaptable, and bioorthogonal click-chemistry. Another recent paper uses a similar approach to conjugate Trastuzumab covalently with a scrambled oligonucleotide, which serves as “sticky nucleotide” [28] for incorporation inside photopolymerized polydiacetylenic micelles. These micelles were subsequently loaded with siRNA against polo-like kinase 1 (PLK1). Notably, at N/P 6, they showed a PLK1 gene-silencing and confirmed cell-selectivity in two different cell models.

In cancer therapies, RNAi effects are advantageous when targeting overexpressed genes in cancer cells. In this study, we target PLK1, known to be overexpressed in various cancer types, including OC [29]. The overexpression of PLK1 resembles a negative prognostic marker for OC patients, associated with short survival and high metastatic rates [30–32]. Many effects of PLK1 are discussed, from its role in epithelial-mesenchymal transition (EMT) to its influence on mitosis and cell checkpoints [33]. It impacts cell metabolism through phosphorylation of CDC25, cyclin dependent kinase I (CDK1) and Cyclin B [34]. The downregulation of PLK1 was shown to induce cell apoptosis, which could be beneficial for the treatment of malignant tumors [35]. PLK1's role was already elaborated *in vivo* in a subcutaneous mouse model, where stable nucleic acid lipid nanoparticles encapsulating siPLK showed promising results, with tumor-derived PLK1 silenced by 45 %. Additionally, PLK1 silencing prolonged median survival from 32 days in the control group to 51 days in the PLK1 group. Of special interest is furthermore PLK1's role in EMT, describing the transition from epithelial-like cells (adherens and tight junctions, apical-basal polarity, cobble stone morphology, and almost no motility [36,37]) to mesenchymal-like cells with spindle-like morphology, front-back polarity, invasive mobility and lacking cell–cell junctions [36,37]. EMT is known to play a crucial role in tumor metastasis and dissemination, driven by agile mesenchymal cells [36]. Decreased cell mobility was observed after downregulation of PLK1 *in vitro* in a cell migration assay. Moreover, patient Kaplan-Meier curves showed that elevated PLK1 levels inversely correlate with melanoma patient survival rates [36]. The researchers reported that the underlying effects stem from previously unknown phosphorylation of the NUMB protein by PLK1, leading to overexpression of EMT-promoting transcription factors including SNAI1 and ZEB1. *Vice versa*, silencing PLK1 via RNAi can downregulate these transcription factors, as investigated here.

After successful uptake of siRNA-mPolyplexes, vector disassembly is crucial for successful gene silencing. To facilitate nanoparticle disassembly and siRNA release, we investigated the effect of introducing disulfide bonds in the linking agent between nanoparticle and targeting ligand as a redox-sensitive nanocarrier. Intracellular high glutathione (GSH) concentrations (2–10 mM) compared to low extracellular concentrations (<10  $\mu$ M) [38,39] may thus enhance transfection efficiencies [40,41].

The aim of this work was to develop a suitable drug carrier formulation for OC treatment. The formulation was initially screened for physicochemical characteristics before applying Design of Experiment (DoE) to further understand formulation aspects. Different hydrophilic/lipophilic balances of underlying PBAEs were screened along with the inclusion or exclusion of disulfide bonds in linking agents. Furthermore, the use of Trastuzumab as a targeting agent was evaluated to determine if it improves nanoparticle uptake and enhances potential OC treatment. After demonstrating proof-of-concept with predefined lead candidates, we investigated their impact on relevant cancer markers, including epidermal growth factor receptor (EGFR) and PLK1. Ultimately, we aimed to assess if cell mobility and EMT behavior can be adjusted following successful PLK1 downregulation via RNAi.

## 2. Materials and methods

### 2.1. Materials

Spermine, OA, *di-tert*-butyl decarbonate, Lipofectamine 2000, OPTI-MEM Serum Reduced Medium, McCoy's 5A (Modified) Medium, 0.25 % Trypsin-EDTA, Alexa Fluor 488 NHS Ester, Alexa Fluor 647 NHS Ester, SYBR Gold Nucleic Acid Gel Stain 10,000X concentrate in DMSO, siRNA against PLK1 (siPLK1), siRNA against EGFR (siEGFR), RNA mini kits, SYBR Green PCR master mix, 4',6-Diamidin-2-phenylindol (DAPI) and Phalloidin/Rhodamin-TRITC reagent were obtained from ThermoFisher Scientific (Schwerte, Germany). 4-(2-hydroxyethyl)-1-piperazineethanesulfonic acid (HEPES), negative control siRNA (siNC), heat inactivated Fetal Bovine Serum (FBS), Penicillin/Streptomycin solution (P/S), Dulbecco's Phosphate Buffered Saline (PBS), Dibenzocyclooctyne-*N*-hydroxysuccinimidyl ester (DBCO-NHS), Accutase solution, Tween 20 and anhydrous dimethyl sulfoxide (DMSO) were purchased from Sigma Aldrich (Darmstadt, Germany). Trastuzumab (Trazimera®) was from Pfizer Pharma (Freiburg, Germany). Amine-modified siRNA for in-house labelling with AlexaFluor NHS esters was obtained from IDT (Integrated DNA Technologies, Inc., Leuven, Belgium). RED-NHS 2nd Generation Protein Labeling Kit was obtained from NanoTemper Technologies GmbH (Munich, Germany) and HER2 was purchased from Sino Biological, Inc. (Beijing, China). 1,4-butanediol diacrylate was purchased from TCI Chemical Industry Co., Ltd. (Tokyo, Japan) and trifluoroacetic acid (99.9%, extra pure) from Acros Organics (Geel, Belgium). Linking agents *N*-((3-Azidopropyl)oxy) carbonyl-3,6,9-trioxadecanedioic acid succinimidyl ester (Azido-PEG3-SS-NHS Ester) and *N*-(Azidopropyl)-3,6,9,12-tetraoxatridecanedioic acid succinimidyl ester (Azido-PEG4-NHS Ester) were both bought from MedChemExpress (Sollentuna, Sweden). For knock-down experiments, high-capacity cDNA synthesis kit was obtained from Applied Biosystems (Waltham, Massachusetts, USA) and both human primers for PLK1 and  $\beta$ -Actin were purchased from Qiagen (Hilden, Germany).

### 2.2. Synthesis of PBAEs

Poly( $\beta$ -amino) esters (PBAE) were synthesized with varying oleylamine (OA) ratios as described previously [10]. Briefly, 1,4-butanediol diacrylate, tri-boc-spermine and oleylamine were dissolved and mixed at 300 mg/mL in dimethyl formamide and reacted at 120 °C for 24 h. Resulting polymers were deprotected using trifluoroacetic acid. Solvent mixtures were evaporated and products were precipitated in pentane three times using acetone before being dried. OA ratios were calculated by <sup>1</sup>H NMR. Polymers were dissolved and stored at -20 °C in anhydrous dimethyl sulfoxide (DMSO) at a concentration of 25 mg/mL. PBAEs with an OA content of 20 % are termed "low OA", those with an OA content of 40 % are "medium OA", and those with an OA content of 68 % "high OA" polymers.

### 2.3. PBAE functionalization

PBAEs were modified to bear azido groups, either with or without an incorporated disulfide group, using NHS-ester chemistry on their primary amines. Two linkers, Azido-PEG3-SS-NHS Ester and Azido-PEG4-NHS Ester were dissolved in anhydrous DMSO and then added dropwise to a 1 mg/mL PBAE solution in 10 mM HEPES pH 7.4 and stirred for 1 h at room temperature. Subsequently, modified PBAEs were purified using 3,000 MWCO spin filters (Sigma Aldrich, Darmstadt, Germany) into 10 mM HEPES pH 5.4. Modified PBAEs were mixed with non-modified PBAEs in a ratio of 1:1 and stored at a concentration of 1 mg/mL in 10 mM HEPES pH 5.4 at -20 °C. In the following, PBAEs, which were modified with Azido-PEG3-SS-NHS Ester, are named with the addition of "SS", indicating the presence of a reducible disulfide bridge.

### 2.4. Trastuzumab functionalization

Trastuzumab was modified with dibenzocyclooctyne (DBCO) according to a method previously published for functionalizing Transferrin and modified accordingly [27]. Briefly, Trastuzumab was dissolved to 10 mg/mL in PBS and stirred. DBCO-NHS was dissolved to 10 mM in anhydrous DMSO and added dropwise to the stirred Trastuzumab solution and reacted for 2 h at room temperature. Trastuzumab-DBCO was purified with 50,000 MWCO (VivaSpin 20, Sartorius Stedim Lab Ltd, Stonehouse, United Kingdom) into 10 mM HEPES pH 7.4 at a concentration of 10 mg/mL. Successful incorporation of DBCO groups was measured spectrophotometrically (NanoDrop One, Thermo Fisher Scientific, Darmstadt, Germany) through assessment of the relative absorbance A280/A309 applying the following formula:

$$\frac{DBCO}{Trastuzumab} = \frac{A309 \times \epsilon_{Trastuzumab}}{(A280 - CF \times A309) \times \epsilon_{DBCO}}$$

where A280 is the absorption value of the sample at 280 nm, A309 is the absorption value of the sample at 309 nm, CF is the correction factor of DBCO at 280 nm (1.089),  $\epsilon_{Trastuzumab}$  is the molar extinction coefficient of Trastuzumab at 280 nm (225,000 M<sup>-1</sup>cm<sup>-1</sup>), and  $\epsilon_{DBCO}$  is the molar extinction coefficient of DBCO at 309 nm (12,000 M<sup>-1</sup>cm<sup>-1</sup>).

### 2.5. Nanoparticle preparation and conjugation

PBAE mPolyplexes were prepared applying a batch-mixing procedure with targeting ligand post-conjugation after particle formation. First, PBAEs and siRNA were diluted to corresponding concentrations applying the following formula for PBAEs:

$$m(\text{polymer}) = n(\text{siRNA}) * M(\text{protonable units of polymer}) * \frac{N}{P} * N^{\circ}$$

(number of siRNA phosphates)

PBAE and siRNA solutions were gently mixed in a 1:1 ratio via pipetting and incubated for 30 min. After incubation, either Trastuzumab or equivalent volumes of formulation buffer were added to the solution to obtain a 1:1 ratio of DBCO to azide. Mixtures were vortexed for 3 s and incubated for another 2 h and then used for subsequent experiments.

### 2.6. Hydrodynamic diameter and zeta potential measurements

The hydrodynamic diameter, polydispersity index (PDI) and zeta potential ( $\zeta$ -potential) were measured using the Zetasizer Advance Ultra (Malvern Instruments, Malvern, UK) following the steps outlined below. For hydrodynamic diameter and PDI measurements using dynamic light scattering (DLS), 100  $\mu$ L of sample were loaded into ZEN0040 disposable cuvettes (Brand GmbH, Wertheim, Germany) and inserted into the device, equipped with a 173° backscatter angle detector. For  $\zeta$ -potential measurements applying Phase Analysis Light Scattering (PALS), samples were diluted with 750  $\mu$ L of 10 mM HEPES pH 5.4 and inserted into the folded capillary zeta cell DTS1070 (Malvern Instruments, Malvern, UK) before measuring. Triplicate measurements were conducted. Refractive index of 10 mM HEPES was determined with a refractometer and set to 1.33, viscosity was set to 0.891 mPa·s, and dielectric constant was set to 79, accurate at a measurement temperature of 25 °C. Data analysis was performed using the ZS Xplorer software (v. 3.31). Results are given as hydrodynamic diameter (nm)  $\pm$  SD for DLS and average charge (mV)  $\pm$  SD for  $\zeta$ -potential.

### 2.7. SYBR gold assay

siRNA encapsulation was determined by SYBR Gold assay as described elsewhere [9]. Briefly, mPolyplexes were prepared at increasing N/P ratios encapsulating 10 pmol siRNA in 20  $\mu$ L of nanoparticle suspension as described earlier. mPolyplexes were transferred to

a black fluorotrac microplate 384-well (Greiner BioOne, Frickenhausen, Germany). 10,000X SYBR Gold stock solution was diluted 2,500-fold with 10 mM HEPES pH 5.4 to obtain a 4X SYBR Gold working solution, of which 6  $\mu$ L were then added to each well and incubated for 5 min in the dark while shaking. Fluorescence intensity was determined using a microplate reader (Tecan Spark, TECAN, Männedorf, Switzerland) at an excitation wavelength of 492 nm and an emission wavelength of 537 nm, with a bandwidth of 20 nm each. Fluorescence intensity of the sample containing no PBAE (N/P = 0) was set mathematically to 0 % encapsulated siRNA. Measurements were performed in triplicates and values are given as mean  $\pm$  SD ( $n = 3$ ).

## 2.8. Design of experiment

A DoE approach was employed to decrease and streamline the number of necessary experiments for nanoparticle cellular uptake assessment from initially 36 to 17 formulations. Additionally, the effects of physicochemical properties such as hydrodynamic diameter and  $\zeta$ -potential were correlated to nanoparticle uptake. The DoE was designed using JMP Pro 17.2.0. software (SAS Institute Inc., Cary, USA). Factors influencing the nanocarrier were selected and are detailed as follows: OA amount and N/P ratio (continuous), targeting ligand, and disulfide bridge (categorical).

## 2.9. Thermal stability of conjugated and unconjugated mPolyplexes

Isothermal DLS (10 acquisitions, 100 % DLS laser intensity) were performed at 25 °C for all mPolyplexes (conjugated and unconjugated) in HEPES buffer (10 mM) at pH 5.4. Briefly, 10  $\mu$ L of mPolyplexes ( $n = 2$ ) were loaded into high-sensitivity capillaries (PR-C006, NanoTemper Technologies GmbH, Munich, Germany) and sealed. The capillaries were transferred to a Prometheus Panta instrument (NanoTemper Technologies GmbH). To explore the temperature-dependent change in mPolyplex size and aggregation behavior, the hydrodynamic radius ( $R_H$ ) and PDI of the nanoparticles were recorded as a function of temperature from 25 °C to 95 °C. The stability of Trastuzumab conjugated nanoparticles was also measured using Nano Differential Scanning Fluorimetry (nanoDSF) by detecting tryptophan fluorescence at 350 and 330 nm and recording the 350/330 nm ratio as a function of temperature from 25 °C to 95 °C. Data analysis was performed using Pr.Panta Analysis (v. 1.4.4).

## 2.10. Binding affinity assay

HER2 was labeled with the Protein Labeling Kit RED-NHS 2nd Generation (cat# MO-L011, NanoTemper Technologies GmbH, Germany). Briefly, 20  $\mu$ M of HER2 (40  $\mu$ L) was incubated with a 3X molar excess of RED-NHS 2nd Generation dye (10  $\mu$ L) in NHS buffer. After 1 h of incubation in the dark, the labeled protein was purified using the B-column of the labeling kit. Protein concentration (920 nM) and degree of labeling (1.2) were determined via UV-Vis absorbance, using the protein extinction coefficient (65,465  $M^{-1} cm^{-1}$ ), the dye extinction coefficient (250,000  $M^{-1} cm^{-1}$ ) and a correction factor of 0.05. Conjugated or unconjugated mPolyplexes were prepared as described earlier with a total of 200 pmol siNC in 100  $\mu$ L of nanoparticle suspension. After the incubation time, 10  $\mu$ L nanoparticles (Ligand) were diluted with 10  $\mu$ L of a 0.02 % Tween 20 solution in 10 mM HEPES pH 5.4. Ligand samples were prepared using 24-point serial dilution with 10  $\mu$ L in each PCR tube. 10  $\mu$ L of target (RED-NHS labeled HER2) at a HER2 concentration of 10 nM (final concentration) were added to each ligand sample.

Samples were transferred to 384 well Dianthus microplates (NanoTemper Technologies GmbH). The measurements were performed using 100 % excitation on a Dianthus instrument at 25 °C using DI. Control software (v 2.1.1). EC<sub>50</sub> values were calculated using DI. Screening analysis software (v 2.1.1). Data was exported and replotted using Python (Matplotlib).

## 2.11. Cell culture

The human ovarian adenocarcinoma cell line SKOV-3 was cultured in McCoy's 5a supplemented with 10 % FBS (growth medium). Cells were cultured in 75 cm<sup>2</sup> flasks (Greiner BioOne, Frickenhausen, Germany) and routinely passaged using 0.25 % trypsin and sterile PBS every 2–4 days when reaching confluency of 80–90 % and constantly kept and maintained in a humidified atmosphere at 37 °C and 5 % CO<sub>2</sub>.

### 2.11.1. HER2 staining

HER2 status of SKOV-3 cells was assessed applying flow cytometry. SKOV-3 cells were seeded at a density of 60,000 cells per well in a 24 well plate (Greiner Bio-One, Frickenhausen, Germany) in 500  $\mu$ L growth medium. After 24 h, cells were washed with PBS and detached using 100  $\mu$ L of Accutase solution per well and incubated for 3–5 min. Accutase reaction was stopped by adding 300  $\mu$ L of fresh growth medium. Cell suspension was transferred to 1.5 mL tubes (Greiner Bio-One, Frickenhausen, Germany) and centrifuged at 400 relative centrifugal force (rcf) for 5 min. Supernatant was aspirated and cells were washed with PBS twice. Following the final wash, the cell pellet was resuspended and stained in either 200  $\mu$ L of antibody solutions prepared according to manufacturer's protocol: HER-2 Monoclonal Antibody (2G11), FITC (Thermo Fisher Scientific, Schwerte, Germany) and the isotype control, Mouse IgG1 kappa (P3.6.2.8.1), FITC (Thermo Fisher Scientific, Schwerte, Germany). The final cell pellet was resuspended in 400  $\mu$ L PBS containing 2 mM EDTA (Sigma Aldrich, Darmstadt, Germany). Stained cells were analyzed using flow cytometry (Attune NxT Flow Cytometer, Thermo Fisher Scientific) with BL-1H to assess HER-2 receptor expression. Results are displayed as histogram plot of one representative sample of three technical replicates ( $n = 3$ ) each.

### 2.11.2. Cellular uptake

For cellular uptake studies, SKOV-3 cells were seeded at a density of 60,000 cells/well in a 24 well plate (Greiner Bio-One, Frickenhausen, Germany) 24 h prior transfection. PBAE mPolyplexes containing 50 pmol siRNA in 100  $\mu$ L formulation buffer were prepared as described above with the addition of 10 % AF488-labelled siRNA, prepared as previously reported [41], and cells were transfected. Lipofectamine 2000 served as positive control, and lipoplexes were prepared according to the manufacturer's instructions, complexing the same amount and composition of siRNA used for mPolyplexes. Additionally, 100  $\mu$ L of 10 mM HEPES pH 5.4 served as blank control. Cells were transferred to 1.5 mL tubes 24 h after transfection using 0.25 % trypsin and washed twice with 400  $\mu$ L PBS in a lab-scale centrifuge at 400 rcf, 5 min, 21 °C. Finally, cells were resuspended in 400  $\mu$ L PBS containing 2 mM EDTA (Sigma Aldrich, Taufkirchen, Germany) for flow cytometry analysis with the Attune NxT instrument (Thermo Fisher Scientific, Darmstadt, Germany) using a 488 nm excitation laser and 530/30 emission filter. Cells were gated according to morphology, and a total of minimum 10,000 viable cells per sample were evaluated. Results are shown as the average median fluorescence intensity (MFI) of three replicates ( $n = 3$ ) in a heat map.

### 2.11.3. EGFR knockdown

The PBAE nanoparticles' capabilities of mediating gene silencing *in vitro* were assessed in a relevant EGFR model. SKOV-3 cells were seeded at a density of 50,000 cells/well in a 24 well plate 24 h prior transfection in growth medium. PBAE mPolyplexes were prepared as described earlier, encapsulating 50 pmol of siRNA either against EGFR (siEGFR) or a negative control siRNA (siNC) in 100  $\mu$ L 10 mM HEPES pH 5.4. Lipofectamine 2000 was used as positive control while cells treated with 10 mM HEPES pH 5.4 or free siEGFR were analyzed for comparison reason. After 48 h of incubation, growth medium was aspirated, and cells were washed with PBS to remove the residual medium. PBS was aspirated, and cells were detached by adding 100  $\mu$ L of Accutase solution per well. After detachment, Accutase reaction was inactivated with 400  $\mu$ L of

growth medium. Cell suspensions were transferred to 1.5 mL tubes and washed twice with PBS by centrifugation at 400 rcf for 5 min. The final washing step was performed by centrifuging for 10 min at 300 rcf. Following the final wash, the cell pellet was resuspended in the antibody solution, prepared as follows: EGFR Antibody, anti-human Vio R667 Reagent (Miltenyi Biotec, Bergisch Gladbach, Germany), was diluted in Magnetic Activated Cell Sorting buffer (MACS buffer, Miltenyi Biotec, Bergisch Gladbach, Germany) 1:200 in a final volume of 100  $\mu$ L, according to the manufacturer's instructions. Each sample was vortexed and incubated for 10 min at 4 °C in the dark. After incubation, cells were washed once by adding 1 mL of MACS buffer and centrifuging for 10 min at 300 rcf. The supernatant was then aspirated, and cell pellets were resuspended in 450  $\mu$ L of MACS buffer. Data analysis was carried out using flow cytometry (Attune NxT Flow Cytometer, Thermo Fisher Scientific, RL-1H excitation and filter). The median fluorescence intensity (MFI) of three replicates per sample ( $n = 3$ )  $\pm$  SD was obtained by analyzing at least 10,000 viable cells.

#### 2.11.4. PLK1 knockdown

The PBAE mPolyplexes' gene silencing capacity was further elucidated in a PLK1 knockdown experiment. SKOV-3 cells were seeded in 24-well plates (Greiner Bio-One, Frickenhausen, Germany) at a density of 50,000 cells per well in 500  $\mu$ L of complete growth medium and incubated for 24 h. After incubation, cells were transfected with nanoparticles containing 100 pmol siRNA either against PLK1 (siPLK1) or a negative control siRNA (siNC), prepared as described above. Lipoplexes with the same amount of siRNA with Lipofectamine 2000 were used as positive control, while cells treated with 10 mM HEPES pH 5.4 served as blank samples. Cells were harvested 24 h after transfection, and RNA was isolated using RNA mini kits according to the manufacturer's instructions. Subsequently, complementary DNA (cDNA) was synthesized from total RNA with a high-capacity cDNA synthesis kit and was then diluted 1:10 for Real Time Quantitative PCR (RT-qPCR) analysis. The RT-qPCR (QuantStudio 3 Real-Time PCR, Thermo Fisher Scientific, Waltham, Massachusetts, USA) was performed using SYBR Green PCR master mix and primers for human PLK1 and human  $\beta$ -actin. Cycle thresholds were acquired by auto-setting with the RT-qPCR software (Thermo Fisher Scientific, Waltham, Massachusetts, USA). The expression of the PLK1 gene's mRNA was normalized to the expression of a housekeeping gene, represented by  $\beta$ -actin applying the  $\Delta\Delta C_t$  method software (Thermo Fisher Scientific, Waltham, Massachusetts, USA). Results are given as mean  $\pm$  SD of biological and technical triplicates ( $n = 3$ ,  $N = 3$ ).

#### 2.11.5. Cell migration assay

For a cell migration assay following PLK1 knockdown, cells were seeded in an ibidi Culture-insert 4 well in  $\mu$  Dish (ibidi GmbH, Gräfelfing, Germany) at a density of 15,000 cells/chamber in 100  $\mu$ L in complete growth medium and incubated for 24 h. After incubation, cells were washed once with PBS and medium was replenished with growth medium and the addition of 1 % P/S. Cells were then transfected with nanoparticles containing 10 pmol siPLK1. Lipoplexes formed with Lipofectamine 2000 served as positive control, while 10 mM HEPES pH 5.4 served as blank control. After transfection, cells were incubated for another 18 h. Afterwards, inserts were carefully removed, and cells were washed three times with PBS and then submerged with growth medium containing 1 % P/S. Pictures of cells migrating towards each other were taken with the EVOS™ M5000 Imaging System (Invitrogen™, Thermo Fisher Scientific, Schwerte, Germany) after 0, 4, 8 and 24 h. Pictures were analyzed with ImageJ Fiji software [42] with the "Wound Healing Size Tool" plug-in. Results were normalized to 100 % wound area at 0 h and are given as % wound area  $\pm$  SD of biological replicates ( $N = 3$ ).

#### 2.11.6. Confocal microscopy images

Nanoparticles' uptake behavior in combination with effects following PLK1 knockdown were further assessed via confocal

microscopy. For this experiment, SKOV-3 cells were seeded into a  $\mu$ -Slide 8 well ibiTreat (ibidi GmbH, Gräfelfing, Germany) at a density of 30,000 cells/well in 200  $\mu$ L growth medium and incubated for 24 h. After incubation, growth medium was aspirated, cells were washed once with PBS and growth medium was replenished. Cells were then transfected with 25 pmol of a 1:1 mixture of siPLK1 and siAF647, encapsulated by mPolyplexes prepared as described earlier. Samples with 10 mM HEPES pH 5.4 served as blank controls. After transfection, cells were incubated for 24 h and then washed three times with 200  $\mu$ L PBS. Following this step, cells were fixed with 4 % paraformaldehyde (4 % PFA) solution and incubated for 15 min in the dark at 4 °C. Next, the PFA solution was aspirated, and cells were washed three times with PBS before applying DAPI at a concentration of 0.5  $\mu$ g/mL in PBS and 1X Phalloidin/Rhodamin-TRITC in PBS to the cells. Cells were incubated for 15 min at 4 °C in the dark and then washed three times with PBS before applying the insert into the confocal microscope (SP-8 inverted confocal microscope, Leica Microsystems, Wetzlar, Germany) with a magnification factor of 40X. Analysis was performed using Leica Application Suite X.

#### 2.12. Statistical analysis

The results are given as mean value  $\pm$  SD unless otherwise stated. One-way ANOVA with a Tukey or Bonferroni Post Test with multiple comparison test was performed by GraphPad Prism software version 9.5.1 (La Jolla, CA, USA) with a 95 % confidence interval.

### 3. Results and discussion

#### 3.1. Physicochemical nanoparticle characterization

PBAEs are well-established as polymeric RNA delivery agents, offering numerous advantages such as adaptability, scalability and the potential for active drug targeting via bioconjugation. In this study, we leveraged these benefits to develop HER2-targeted mPolyplexes encapsulating siRNA. We initially modified the PBAE backbone recently developed by our group, which was characterized by a high encapsulation rate, low cytotoxicity, and superior transfection efficiency [10,14,43]. The PBAE backbone contains spermine as cationic part for RNA complexation via electrostatic interactions, and oleylamine as hydrophobic component, facilitating endosomal escape [14]. We recently optimized synthesis parameters applying DoE to better understand the block polymerization reaction [10]. Following the successful synthesis of various % OA PBAEs, these drug carriers were further modified towards an azide-bearing function utilizing the primary amine function in the spermine pendent chains through NHS ester chemistry. Similarly, the mAb Trastuzumab was modified to introduce an alkyne-bearing group, incorporated inside the DBCO group, as verified spectrophotometrically. Click chemistry serves as a versatile tool for attaching targeting ligands due to its bioorthogonality [44]. By modifying both, PBAE and Trastuzumab, we were able to apply SPAAC after nanoparticle formation. This concept was previously established and reported by our group with LNPs and Transferrin [27]. A schematic representation of the nanoparticle formation workflow is provided in Fig. 1.

To assess the suitability of nanoparticles for further experiments, hydrodynamic diameter, polydispersity index (PDI), and  $\zeta$ -potential were determined in a comprehensive screening of our selected formulations using DLS and PALS (Fig. 2).

By focusing first on the low OA PBAE, it was observed that all nanoparticles formulated at N/P 5 exhibited hydrodynamic diameters exceeding 250 nm. Interestingly, the  $\zeta$ -potential revealed a noteworthy trend: nanoparticles formulated at N/P 5 without Trastuzumab had a negative  $\zeta$ -potential, while their targeted counterparts exhibited a positive  $\zeta$ -potential. This can be attributed to the isoelectric point (IP) of Trastuzumab, which is approximately 9.2 [45]. At the relevant pH, Trastuzumab is positively charged, explaining the shift in  $\zeta$ -potential. Moreover, this indicates successful conjugation of the monoclonal

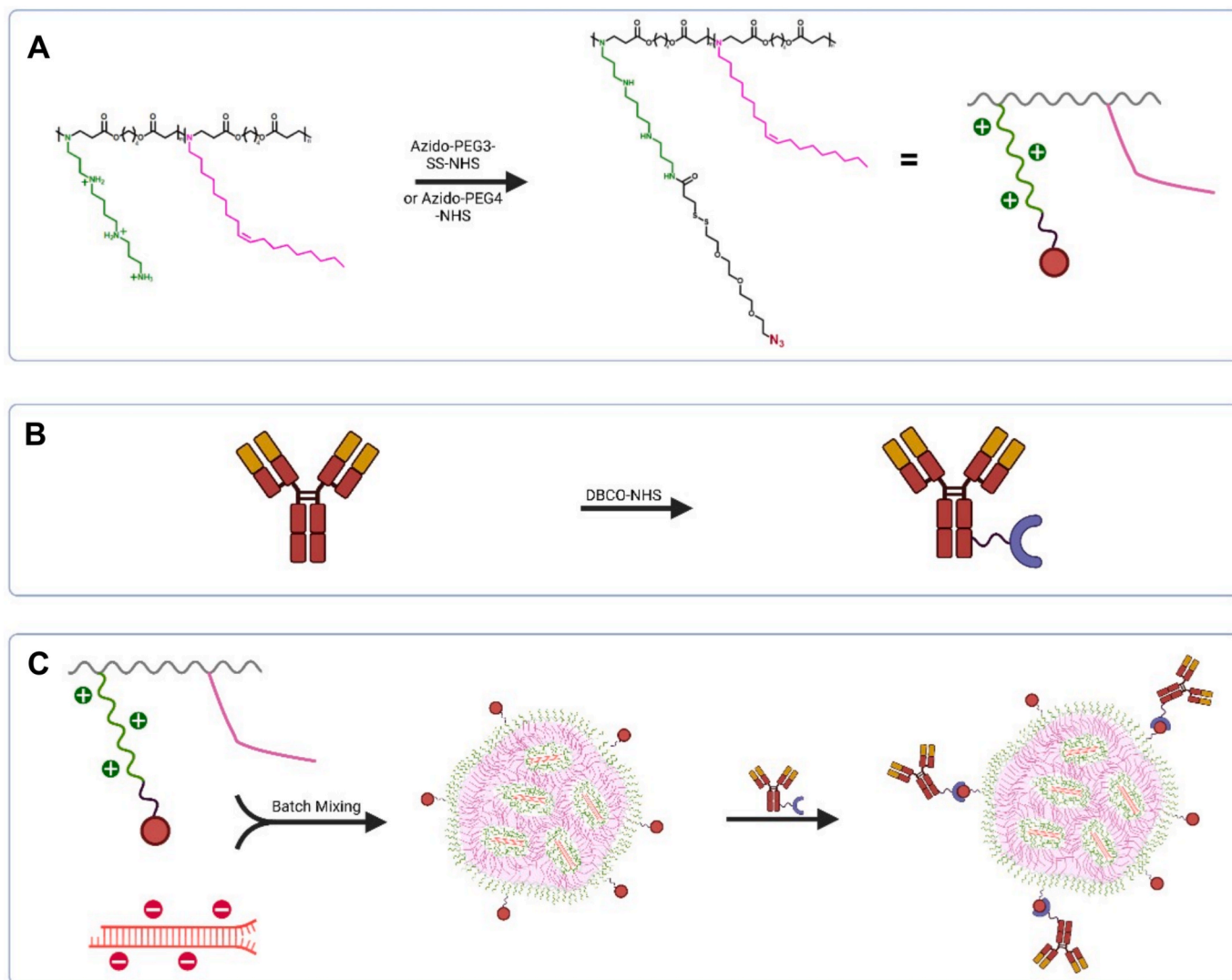


**Fig. 1.** Schematic representation of nanoparticle formulation. A) PBAE modification towards azide-bearing groups (the structure depicted here represents only one of the two described versions of the linking agent). B) Trastuzumab modification towards alkyne-bearing group. C) Nanoparticle formation and post-insertion functionalization with the targeting ligand.

antibody to the preformed nanoparticles using click-chemistry. The sizes remained smaller, ranging from 50 to 200 nm, for higher N/P ratios of the low OA PBAE. However, especially at N/P 15, considering the high PDI, these data should be interpreted only with caution.

Nanoparticles formulated with medium OA PBAE were overall in the expected and acceptable size range of approximately 50 nm for N/P ratios of 10 and 15, and slightly larger, up to 200 nm, at N/P 5. Notably, the PDI here was overall lower, indicating a more monodisperse formulation. The incorporation of lipophilic OA moieties resulted in more condensed and well-defined nanoparticles, as already simulated by Steinegger et al. [43]. The  $\zeta$ -potential of these formulations was slightly positive, ranging from 5 to 35 mV, making them suitable for cellular uptake without causing high toxicity.

High OA PBAE nanoparticles exhibited the best physicochemical characteristics regarding hydrodynamic diameter, PDI, and  $\zeta$ -potential. While an aggregation phenomenon occurred for the PBAE-Azide at N/P 10 with a hydrodynamic diameter of approximately 400 nm, this can be explained by the  $\zeta$ -potential being close to 0 mV. For other formulations, sizes ranged from 50 nm to 200 nm with an overall low PDI. Particularly, all formulations measured at N/P 15 exhibited a PDI < 0.2, indicating nanoparticle populations with a narrow size distribution and further supporting the hypothesis that high OA PBAEs form more globular

nanoparticles [43]. For  $\zeta$ -potential, similar trends were observed with respect to the IP of trastuzumab, making targeted nanoparticles more positive than their azide counterparts.

The encapsulation efficiency of siRNA, determined via SYBR Gold assay, also showed promising results. All formulations, except for high OA PBAE N/P 5, had an siRNA encapsulation efficiency above 98 %. For high OA PBAE N/P 5, it is assumed that an insufficient number of protonated amines was present to facilitate complete encapsulation.

Overall, the physicochemical characteristics of nanoparticles, especially for medium and high OA PBAEs, were satisfactory, with sizes in the range of 50 – 200 nm, making them suitable for passing through fenestrated endothelium and thus benefiting from the EPR effect [19,46].

### 3.2. Design of experiment

Design of Experiment (DoE) is a powerful tool for systematic and simultaneous screening of a variety of variables. Unlike the traditional “trial-and-error” or complete screenings, the DoE approach can identify optimal desirability for one or more goals. By utilizing a complex design space, it can derive findings with a minimal number of necessary experiments [47,48]. This makes it a highly time- and cost-efficient

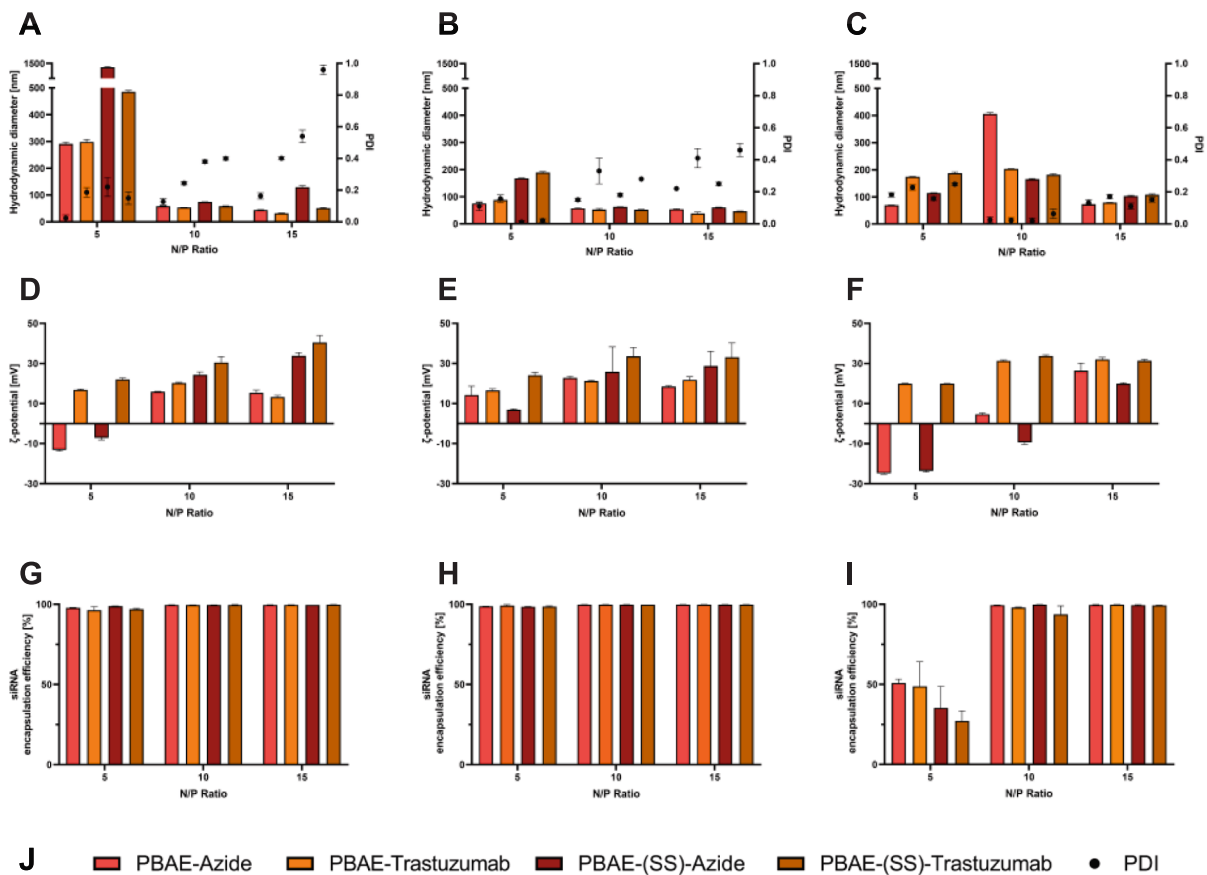


**Fig. 2.** Physicochemical characterization of PBAE nanoparticles either as PBAE-Azide (red), PBAE-Trastuzumab (orange), PBAE-SS-Azide (dark red) or PBAE-SS-Trastuzumab (dark orange) in N/P ratios ranging from 5 to 15. The left column (A, D, G) represents 20 % (= low) OA PBAE, the middle column (B, E, H) the 40 % (= medium) OA PBAE and the right column (C, F, I) the 68 % (= high) OA PBAE, whereas Fig. 2J serves as color legend. Results are given as mean ± SD of three replicates (n = 3). (For interpretation of the references to color in this figure legend, the reader is referred to the web version of this article.)

approach, advantageous for the screening of high-value resources and thus suitable for pharmaceutical drug development. Additionally, through matching mathematical models, it provides researchers with insights into which screened variables significantly impact the pre-set goals. Moreover, it can predict the impact of two initial independent variables as a sum of each other [48]. For a more mechanistic insight into the development of DoE studies for drug development, the reader is referred to [47].

By adopting a DoE approach set up using the JMP Pro 17 software, the number of required experiments to screen all four variables (% OA PBAE, N/P ratio, disulfide bridge and targeting ligand) was reduced from 36 to 17, thereby more than halving the initial number. The chosen formulations are listed in Table 1. Initially, physicochemical parameters obtained in Section 3.1 were listed and plotted against acquired nanoparticle uptake data (Supplementary Fig. S1). From this data set, the model predicted the best-performing agent, which was together with the two best-performers out of the above list analyzed further for receptor binding and knockdown experiments.

3.3. Cellular uptake

Cellular uptake studies were conducted to evaluate the ability of (targeted) PBAE nanoparticles to be internalized by SKOV-3 cells applying flow cytometry. First, positive HER2 receptor status was confirmed, as shown in Fig. 3A. While blank and isotype control samples exhibited no secondary antibody binding, the cells treated with the anti-HER2 primary antibody showed binding. This indicates a positive HER2 receptor status in the SKOV-3 cells used, which is in line with findings

**Table 1**  
Design of Experiment formulations with different factors.

	% OA PBAE	Targeting Ligand	Disulfide Bond	N/P Ratio
DoE 1	68	Yes	No	10
DoE 2	40	Yes	Yes	10
DoE 3	68	Yes	Yes	5
DoE 4	68	No	No	15
DoE 5	68	Yes	Yes	15
DoE 6	20	No	No	10
DoE 7	40	No	No	10
DoE 8	68	No	Yes	10
DoE 9	20	No	Yes	5
DoE 10	68	No	No	5
DoE 11	40	Yes	No	15
DoE 12	20	Yes	No	15
DoE 13	40	Yes	No	5
DoE 14	20	Yes	Yes	10
DoE 15	20	No	Yes	15
DoE 16	40	No	Yes	10
DoE 17	20	Yes	No	5

from literature [3]. Generally speaking, the SKOV-3 cell line is a widely used model for studying OC [31,49–51], which is why it was chosen for this experimental series.

Subsequently, nanoparticles were screened according to the DoE space elaborated in Section 3.2. For better visualization of the DoE methodology, all possible formulations are depicted in Fig. 3B, while the actual experiments performed and their corresponding MFI values are presented in a heat map.

As shown in Fig. 3B, successful nanoparticle uptake was observed,

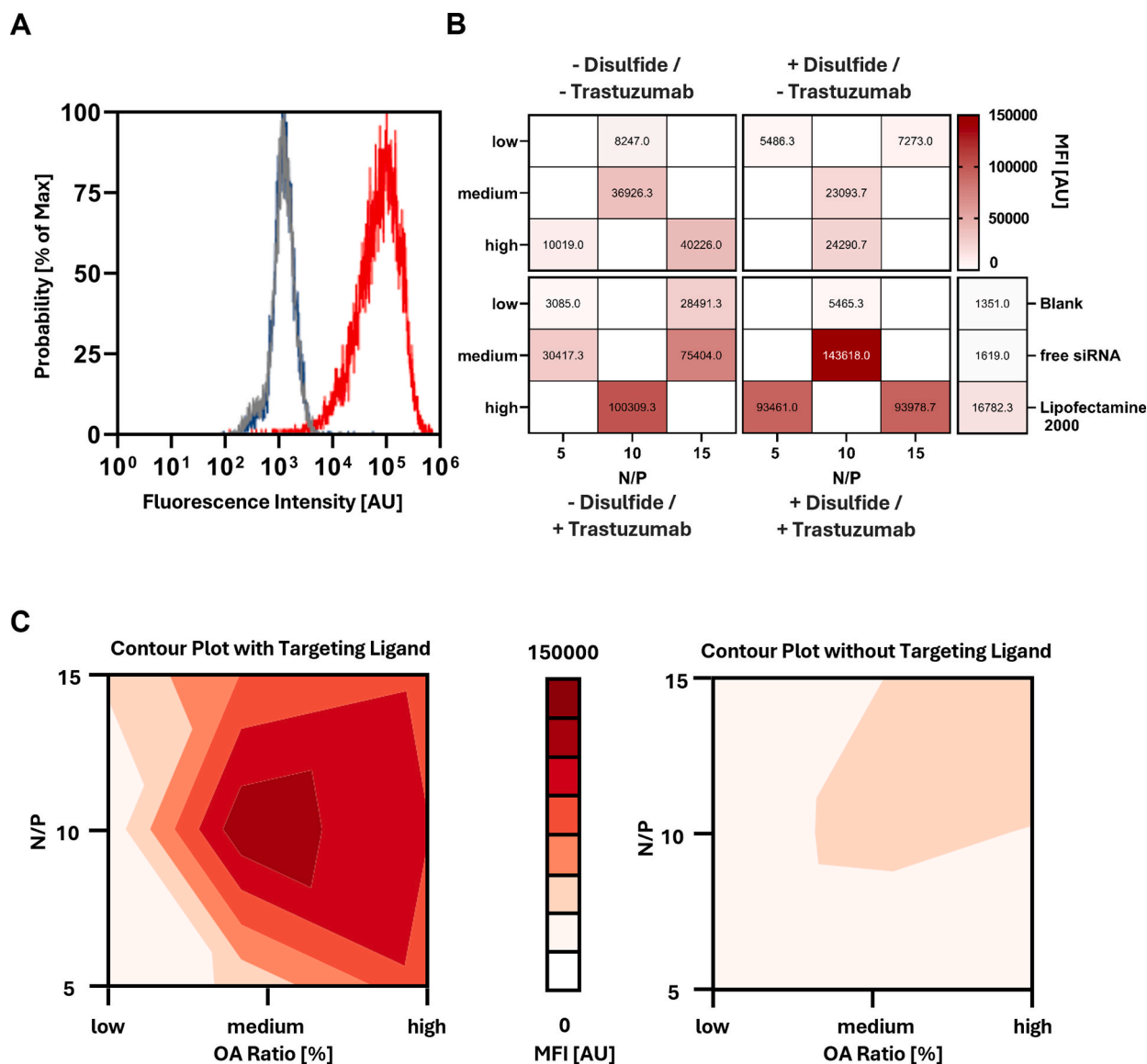


**Fig. 3.** Cellular uptake experiment in SKOV-3 cells, transfected with 50 pmol of siRNA containing 90 % siNC and 10 % siAF488 24 h before harvesting for subsequent flow cytometry analysis. A) HER2 receptor staining histogram plot with blank samples in grey, Isotype control samples in blue and HER2-antibody samples in red. B) Results of cellular uptake experiments in SKOV-3 cells, visualized in a heat map and MFI data; AU = arbitrary unit. C) Illustration of cellular uptake in contour plot, dividing the group with targeting ligand (Trastuzumab) and without targeting ligand. Results in B) are given as mean of the Median Fluorescence Intensity (MFI) of three replicates ( $n = 3$ ). (For interpretation of the references to color in this figure legend, the reader is referred to the web version of this article.)

with values peaking above 140,000 MFI. The incorporation of a disulfide bond within the linking agent appeared to have no significant influence on nanoparticle uptake (Supplementary Fig. S2). When examining the influence of Trastuzumab, a clear trend was evident in both the heat map and in the contour plot in Fig. 3C: the addition of Trastuzumab enhanced nanoparticle uptake. This enhanced uptake is attributed to the interaction with HER2, facilitating the internalization of targeted nanoparticles within cells [18]. This trend is statistically significant, as illustrated in the effect summary in Supplementary Fig. S2.

Another factor analyzed was the % OA PBAE and the N/P ratio. While no observable benefit was found among different N/P ratios, the trend for selecting the % OA PBAE was shifted in favor of the high OA PBAE, which is also supported by the effect summary (Supplementary Fig. S2). A third significant effect was the interaction between the % OA PBAE and the targeting ligand, indicating that these two factors are interdependent. Overall, as can be seen in the predicted against actual nanoparticle uptake plot (Supplementary Fig. S3), a good mathematical correlation was achieved. Based on these results, the DoE model was

used to maximize each factor for optimal cellular uptake. As can be seen in the prediction profiler (Supplementary Fig. S4), DoE2 was identified as positive outlier and therefore not equally considered in the prediction model for enhanced uptake. The resulting prediction suggested the following formulation: 68 % OA PBAE, N/P 15, with targeting ligand, which resembles DoE5. To compare the predicted best-performer, the next two best-performing formulations, DoE1 and DoE2, were included to further verify these findings and are subject to the following experiments.

### 3.4. Thermal stress analysis of mPolyplexes

Nanoparticles were evaluated for their thermal stability and size dependent colloidal stability of Trastuzumab conjugated mPolyplexes. Fig. 4A shows nanoDSF unfolding curves of the mPolyplexes with and without Trastuzumab for DoE1, DoE2 and DoE5. All nanoparticles conjugated with Trastuzumab show inflection temperatures around 69 °C, closely matching that of Trastuzumab only (70 °C). This confirms

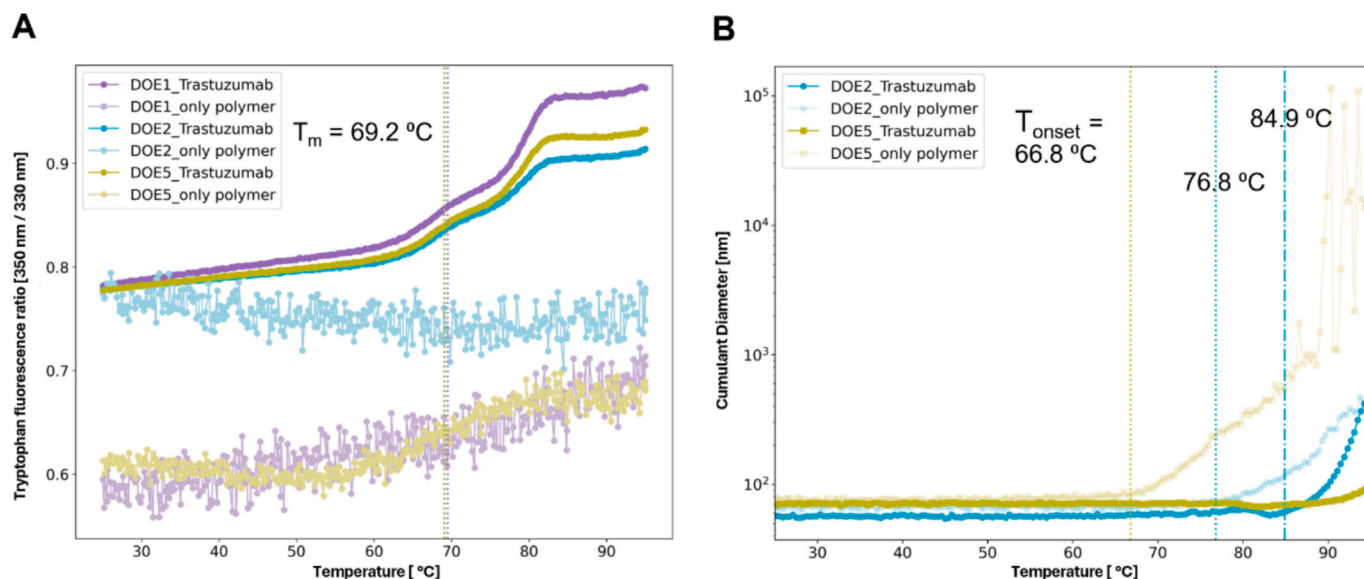


**Fig. 4.** Thermal stress analysis of mPolyplexes. A) Thermal stability of nanoparticles with and without Trastuzumab. B) Temperature dependent colloidal stability of mPolyplexes with Trastuzumab (solid blue and yellow curves) and without Trastuzumab (transparent blue and yellow curves) for DoE2 and DoE5. (For interpretation of the references to color in this figure legend, the reader is referred to the web version of this article.)

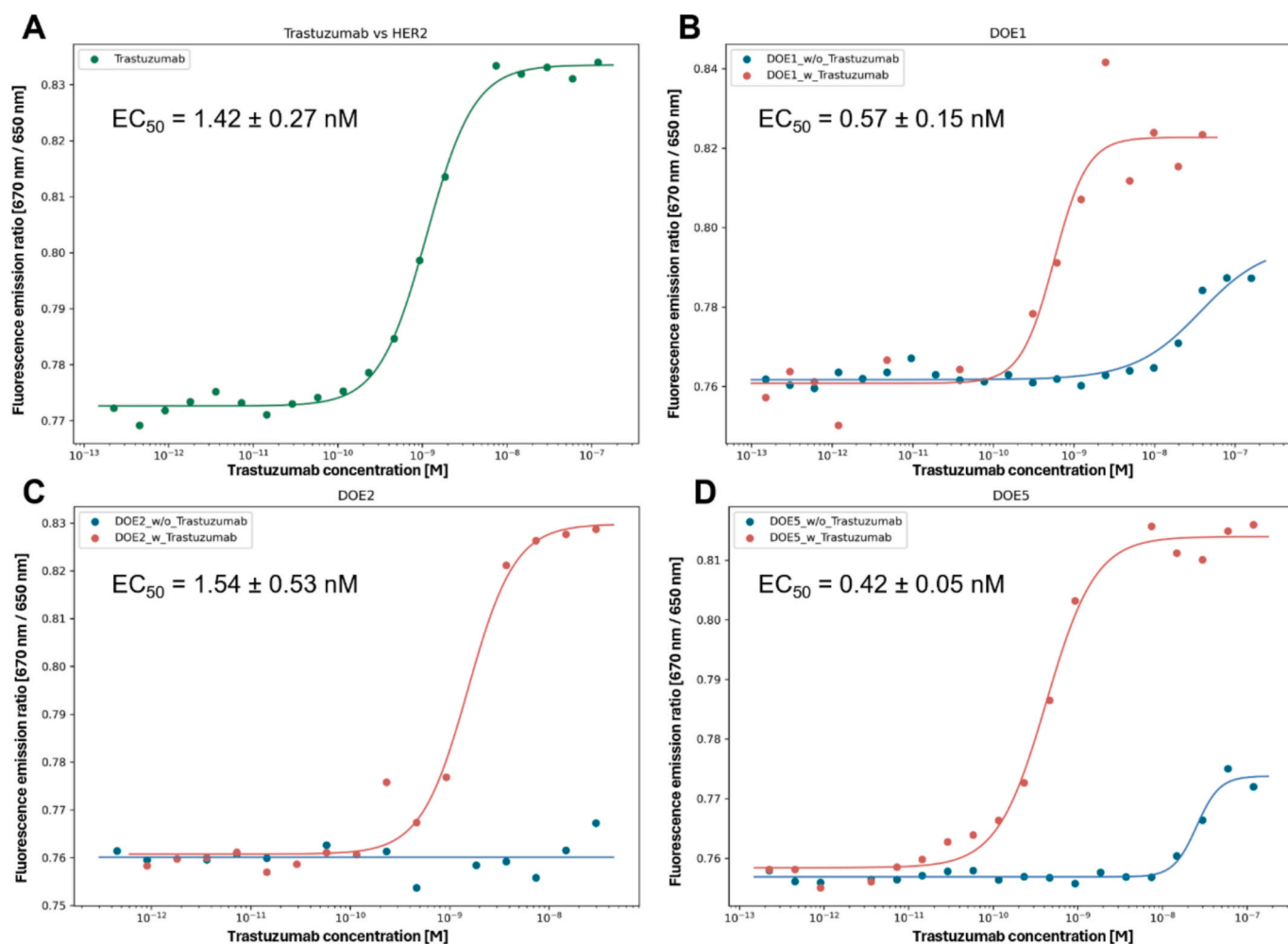


**Fig. 5.** Spectral shift dose-response curves of A) Trastuzumab only, B) DoE1, C) DoE2 and D) DoE5, together with their negative controls against labeled HER2. Assays were performed in HEPES buffer at a 10 nM concentration of HER2. Lines are theoretical and described by the Hill equation, with fitting parameter  $EC_{50}$  reported in the figure panel.

thermal stability of Trastuzumab within the mPolyplex. Fig. 4B shows the temperature-dependent colloidal stability of DoE2 and DoE5 with and without Trastuzumab. While DoE1 showed similar thermal unfolding behavior, DLS data analysis revealed a pronounced increase in particle size (Supplementary Fig. S5), indicating aggregation; therefore, its size profile is excluded from Fig. 4B. However, for both DoE2 and DoE5, the incorporation of Trastuzumab into the mPolyplexes increased their colloidal stability. As seen from the thermal stress test, the onset temperature is higher for DoE2 with Trastuzumab (blue dashed lines) compared to DoE2 without Trastuzumab (blue dotted lines). Similarly, for DoE5, the formulation with Trastuzumab (yellow dashed lines) does not exhibit a significant increase in particle size across the temperature range, resulting in the absence of a defined onset temperature, suggesting much higher colloidal stability compared to DoE5 without Trastuzumab (yellow dotted line).

### 3.5. Binding assay

Spectral shift binding assays were employed to investigate the binding interaction between HER2-targeted mPolyplexes with labeled HER2 (RED-NHS 2nd Generation dye) using Dianthus (NanoTemper Technologies GmbH). This fluorescence-based biophysical technique analyzes molecular interactions by detecting wavelength shifts in the emission spectrum of a fluorophore attached to the target molecule upon ligand binding. During the binding event, changes in the fluorophore's chemical environment cause a shift in its emission wavelength. In this study, emission was detected at two distinct wavelengths (670 nm and 650 nm). The ratio of these intensities (670 nm/650 nm), referred to as the spectral shift ratio, was used to determine affinity parameters such as the dissociation constant ( $K_d$ ) and  $EC_{50}$  [52].

We tested all three different DoE-predicted formulations with different polymer compositions containing Trastuzumab. Nanoparticles were also formed without Trastuzumab for comparison with their respective DoE-predicted formulations. Fig. 5 shows the dose-response curves for Trastuzumab (positive control), DoE-predicted formulations with and without Trastuzumab with labeled HER2. All the DoE-predicted formulations exhibit clear binding with labeled HER2, whereas no binding was detected for DoE-predicted formulations without Trastuzumab at similar polymer concentrations. The binding affinity of DoE2 and DoE5 showed  $EC_{50}$  value around 1.54 nM and 0.42 nM (Fig. 5C and D), close to the  $EC_{50}$  value obtained for HER2-trastuzumab (1.42 nM, Fig. 5A) interaction. Although a binding curve was evident for DoE1 (Fig. 5B), given the sample was aggregated (Supplementary Fig. S5),  $EC_{50}$  should be treated with caution. Furthermore, at higher concentrations of mPolyplexes containing Trastuzumab, we observed a second binding region (Supplementary Fig. S6) for DoE2 and DoE5. We attribute this to non-specific binding of nanoparticles to HER2, likely driven by the larger particle size (compared to only Trastuzumab) at higher concentrations. Similar binding was also observed for mPolyplexes lacking Trastuzumab in DoE2 and DoE5, further supporting the role of size-induced nonspecific interactions.

### 3.6. EGFR knockdown

After confirming successful nanoparticle uptake and HER2-receptor binding affinity, knockdown efficiency in a relevant epidermal growth factor receptor (EGFR) model using SKOV-3 cells was investigated. EGFR, a tyrosine kinase, is known to play a crucial role in various cancer types including non-small cell lung cancer (NSCLC), but also OC [33,53]. Alongside PLK1, EGFR promotes cell migration and proliferation and is associated with poor disease prognosis. Furthermore, as it is expressed on the cell surface, it is eligible for knockdown screening applying flow cytometry. DoE 1, 2, and 5 formulations were analyzed for EGFR knockdown efficacy after siEGFR transfection by comparing them with their scrambled corresponding siNC group. Furthermore, to evaluate the targeting strategy, in both versions either siEGFR or siNC, the

targeting ligand Trastuzumab was either added or excluded. In Fig. 6A, the schematic workflow of the experiment is visualized. Figs. 6B–D represent the results for DoE1, DoE2, and DoE5, respectively.

Fig. 6B demonstrates that the positive control, Lipofectamine 2000, reached an EGFR knockdown of nearly 80 %. For the untargeted DoE1 formulation, an even higher knockdown result of around 82 % was obtained. However, when the targeting ligand was attached, the gene silencing efficiency was decreased to 62 %. The lower EGFR expression observed for the siEGFR sample compared to siEGFR with attached Trastuzumab was unexpected in DoE1 and cannot be explained by the overall positive effect on nanoparticle uptake. Interestingly, and consistent across all different DoE formulations, the siNC samples also led to some extent of EGFR suppression. This could be attributed to non-specific binding towards receptor proteins, as observed in the HER2 binding assay. Nevertheless, the sequence-specific effect was consistently and significantly better than the scrambled counterpart. For DoE2 and DoE5, similar trends were observed: non-specific downregulation of EGFR from siNC samples, which were both significantly surpassed by the siEGFR samples. Additionally, for the Trastuzumab-targeted samples, an siRNA sequence specific knockdown was observed. Overall, the best gene silencing efficiency among all samples in this experiment was from the Trastuzumab-targeted DoE5 siEGFR samples, with knockdown levels exceeding 80 %, thereby surpassing Lipofectamine 2000 and emerging as our lead candidate for further experiments. This finding furthermore reflects the results of previous binding assays.

As EGFR *per se* resembles a potential target for treating OC, these results are promising, demonstrating high knockdown efficiency in a relevant model. However, to further validate the PBAE's potential in a relevant set-up, another disease-related target, namely PLK1, was selected for further evaluation.

### 3.7. PLK1 knockdown via RT-qPCR

Successful gene silencing of a selected, ovarian-cancer related, target PLK1 was confirmed in a SKOV-3 cell model using RT-qPCR, as can be seen in Fig. 7. This figure compares the mRNA levels of the target mRNA PLK1 with the housekeeping mRNA  $\beta$ -Actin, applying the  $\Delta\Delta Ct$  method. The positive control, Lipofectamine 2000, exhibited a gene silencing efficacy of 65 %. Interestingly, our PBAE nanoparticles in both, untargeted DoE5 and targeted DoE5, performed slightly better with values of 69 % and 70 %, respectively. Considering Lipofectamine's toxicity, which renders it unsuitable for *in vivo* applications, these results are promising for further evaluation. However, Trastuzumab targeting did not demonstrate an additive effect on gene silencing efficacy, most likely due to the already high gene silencing efficacy values of the untargeted version and the high dose of siRNA in this experiment. Interestingly, a targeting effect on the gene silencing level was observed with lower siRNA doses and longer incubation times, as shown in Supplementary Fig. S7. In contrast, siNC samples did not show any knockdown of PLK1. This finding highlights the sequence specific siRNA effect. Surprisingly, even a slight increase in PLK1 abundance was observed for untargeted DoE5 (9 %) and for targeted DoE5 (35 %) samples. This experiment demonstrates that our developed siRNA nanocarrier can effectively silence a relevant target that plays an important role in the development of ovarian cancer. For instance, it can be hypothesized that downstream effects of PLK1 were further suppressed. To further evaluate these downstream effects on cell mobility and morphology, additional cell migration and confocal microscopy experiments were conducted.

### 3.8. Cell migration assay

As described earlier, PLK1 plays an important role in cell cycle progression as well as in cell migration and EMT. While high abundance in PLK1 is linked to higher cell migration and invasion, its knockdown has already been shown to hinder the former [36,54]. To evaluate whether PLK1 gene silencing through PBAE mPolyplexes can influence

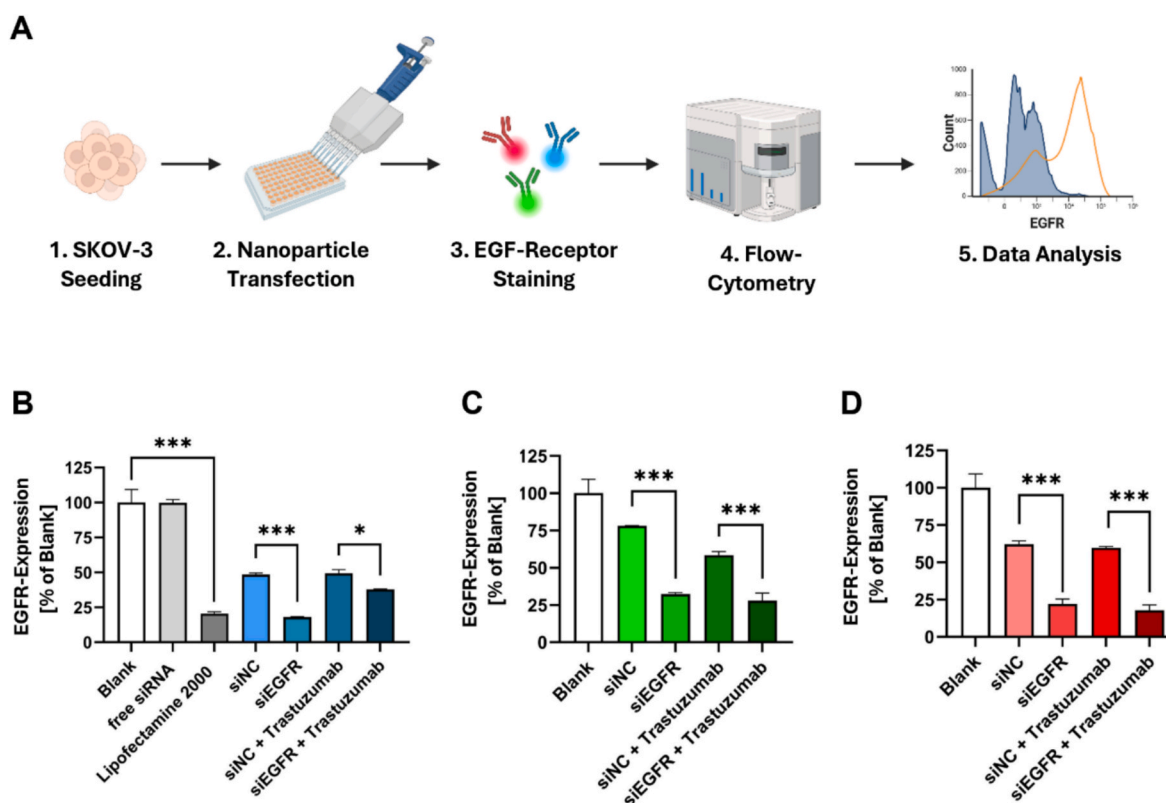


**Fig. 6.** EGFR knockdown experiment in SKOV-3 cells. Cells were transfected with 50 pmol either siNC or siEGFR at the respective N/P ratio of the corresponding DoE trial. After 24 h of incubation, cells were harvested, EGFR stained and subjected to flow cytometry analysis. A) Schematic representation of experimental workflow. Results are given as % EGFR expression of blank samples determined via flow-cytometry of B) DoE1, C) DoE2 and D) DoE5. (Data are showing mean  $\pm$  SD,  $n = 3$ ; Statistical analysis was performed via One-way ANOVA, \*,  $p < 0.05$ , \*\*\*,  $p < 0.001$ ; each versus indicated control groups).

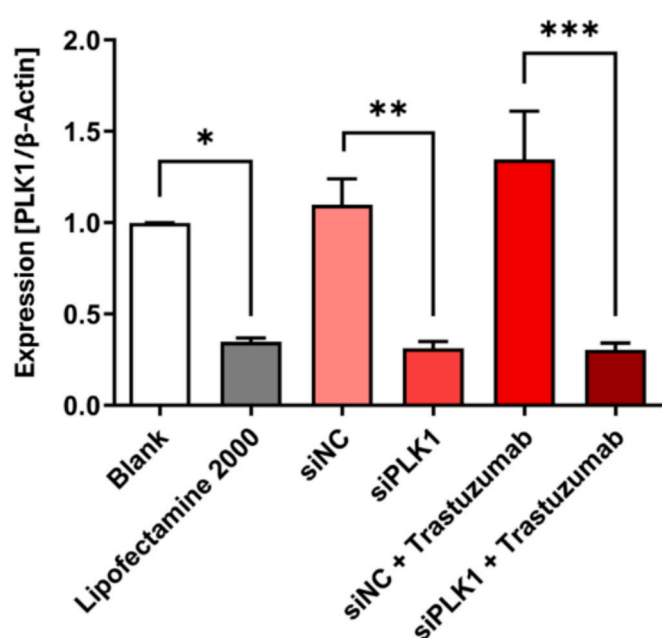


**Fig. 7.** PLK1 knockdown in SKOV-3 cells transfected with DoE5 formulation encapsulating 100 pmol of either siNC or siPLK1 for 24 h. PLK1 expression was evaluated applying RTqPCR by comparing PLK1 mRNA levels against the house-keeping  $\beta$ -Actin mRNA levels. (Data are showing mean  $\pm$  SD,  $N = 3$ ; Statistical analysis was performed via One-way ANOVA, \*,  $p < 0.05$ , \*\*,  $p < 0.01$ , \*\*\*,  $p < 0.001$ ; each versus respective control groups).

those factors, a cell migration assay was conducted, as depicted in Fig. 8 and Supplementary Fig. S8. As shown in Fig. 8, samples were normalized to 100 % wound area at  $t = 0$  h. Blank samples constantly decreased wound area over the next 24 h, resulting in almost complete confluency after 24 h (wound area = 2 %). In samples transfected with either Lipofectamine 2000 or the DoE5 formulation, either without or with Trastuzumab, the wound closure progressed much slower, with values decreasing only down to 72 %, 68 % and 80 %, respectively. These findings are in line with the previously shown PLK1 and EGFR knockdown results. Through transfection with the developed mPolyplexes, a change in cellular macroscopic behavior in terms of motility was achieved. This further supports the role of PLK1 in this process [54]. The inhibition of cell migration can play a crucial role in avoiding tumor dissemination and metastasis and is therefore a pivotal component of a possible OC therapy.

### 3.9. Confocal microscopy of PLK1 knockdown

For visualization of improved nanoparticle uptake through the targeting ligand as well as the ability of gene silencing of PLK1 causing a subsequent macroscopic change in cell behavior, confocal images were taken. As shown in Fig. 9A, blank SKOV-3 cells exhibit mesenchymal characteristics, as highlighted by white arrows. Filamentous actin, a part of the cell cytoskeleton, is visualized in green. In Fig. 9A, more cells appear in a fibroblast-like morphology with an elongated front-back polarity [37,55]. In contrast, Fig. 9B shows PBAE mPolyplex uptake by siRNA signals inside the cells, visualized in magenta. Additionally, the cellular behavior changed in that regard that mesenchymal structures transformed into epithelial-like structures. For the targeted PBAE mPolyplexes (Fig. 9C), it can be found that a much more pronounced nanoparticle uptake occurred, with higher intensity in magenta

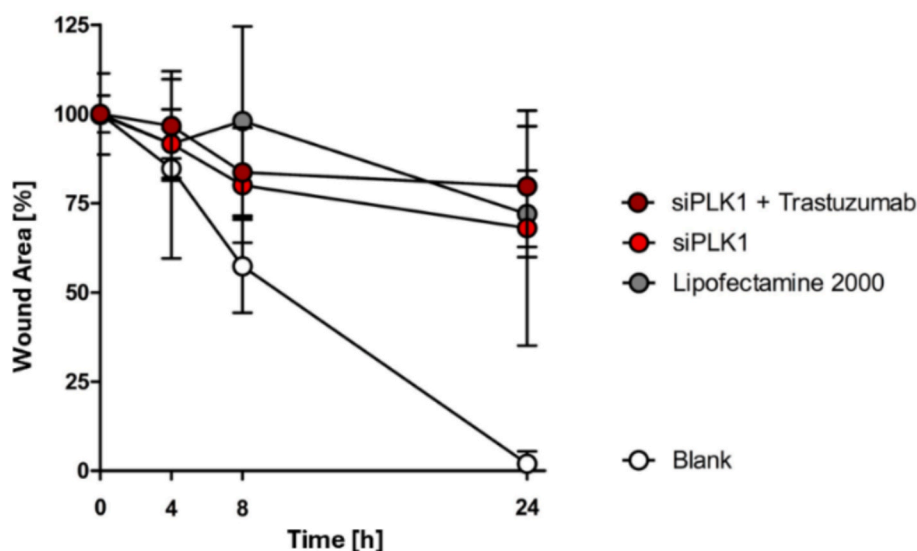


**Fig. 8.** Migration Assay of SKOV-3 cells cultured in an ibidi Culture-insert 4 well in  $\mu$  dish and transfected with 10 pmol siPLK1 and incubated for 24 h. Resulting % wound area was observed over the following 24 h and calculated with ImageJ Fiji Software. (Data are showing mean  $\pm$  SD, N = 3).

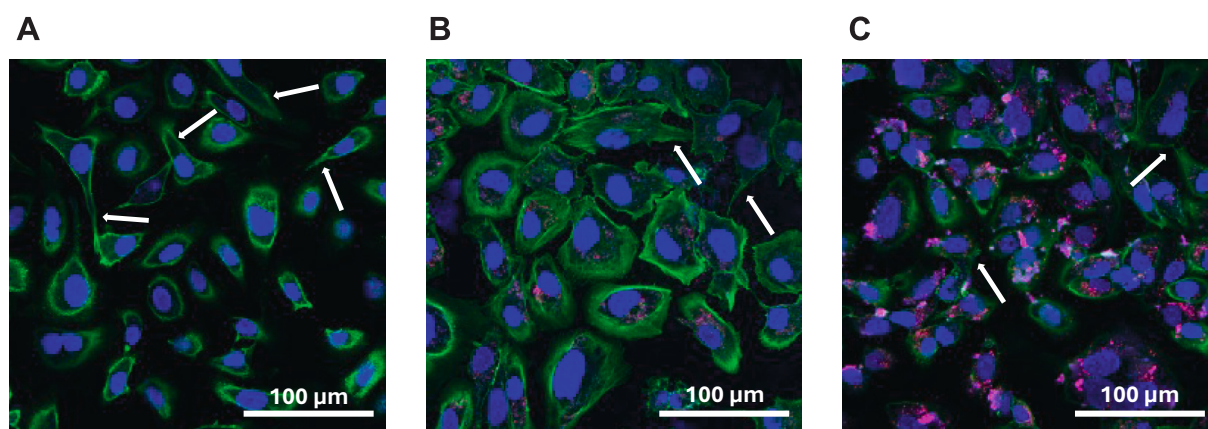


**Fig. 9.** Cellular Uptake and PLK1 knockdown evaluated with confocal microscopy images of SKOV-3 cells transfected either with formulation buffer only (A) or with 25 pmol siRNA, which consisted to 50 % of siAF647 and 50 % of siPLK1, encapsulated by untargeted DoE5 (B) or targeted DoE5 (C). All samples were stained with 0.5  $\mu$ g/mL DAPI (blue) and 1X Phalloidin/Rhodamin-TRITC (green). Fluorescent siRNA is visualized in magenta. (For interpretation of the references to color in this figure legend, the reader is referred to the web version of this article.)

compared to Fig. 9B. This finding supports the previously reported benefit of the targeting ligand Trastuzumab toward nanoparticle uptake, as discussed in Section 3.3. Beyond that and comparable to Fig. 9B, fewer mesenchymal structures were observed in comparison to blank cells. It can be hypothesized, along with results from the cell migration assay, that cells transfected with siPLK1 have a lower tendency for mesenchymal movement and decreased cell motility [32]. This finding further supports the hypothesis that our PBAE drug delivery system can efficiently knockdown PLK1, leading to favorable macroscopic changes that could be beneficial in OC treatment.

#### 4. Conclusion and outlook

Often-cited PBAEs have been in constant focus of RNA researchers since the beginning of this millennium. Our group has successfully improved the initial molecular structures, optimizing hydrophilic/lipophilic balance and RNA encapsulation at low N/P ratios. In this study, we further modified resulting mPolyplexes to create a targeted drug carrier against HER2-overexpressing cells or tissues with Trastuzumab.

Through the thoughtful application of Design of Experiment, we devised an advanced formulation aimed to achieve high cellular uptake following HER2 internalization, which even surpassed that of commercially available Lipofectamine 2000. Gene silencing activity of relevant genes in the progression of OC was satisfactory, with knockdown values exceeding 70 %. SKOV-3 cells exhibited positively changed behavior after PLK1 knockdown in terms of cell migration and EMT.

However, further research is needed to investigate the influence of Trastuzumab targeting on knockdown efficacy via PBAE mPolyplexes, as well as to evaluate their performance *in vivo* in a suitable mouse model. These findings should lay the foundation for further research towards the development of applicable OC treatments using RNAi.

#### Declaration on the use of Artificial Intelligence models in the writing process

This manuscript was developed with the assistance of Microsoft Copilot, an AI language model, to enhance the scientific language. The authors confirm that all findings and interpretations are their own.

## CRediT authorship contribution statement

**Joschka T. Müller:** Writing – original draft, Visualization, Validation, Methodology, Investigation, Formal analysis, Data curation. **Salvatore Caruso:** Investigation, Formal analysis. **Anny Nguyen:** Methodology, Investigation, Formal analysis. **David C. Jürgens:** Visualization, Investigation, Data curation. **Adrian P.E. Kromer:** Investigation, Formal analysis. **Sahana Sheshachala:** Software, Resources, Methodology, Funding acquisition, Formal analysis. **Nathan B.P. Adams:** Resources, Project administration, Methodology, Funding acquisition. **Olivia M. Merkel:** Writing – review & editing, Supervision, Resources, Project administration, Funding acquisition, Conceptualization.

## Declaration of competing interest

The authors declare that they have no known competing financial interests or personal relationships that could have appeared to influence the work reported in this paper.

## Appendix A. Supplementary material

Supplementary data to this article can be found online at <https://doi.org/10.1016/j.ejpb.2025.114904>.

## Data availability

Data will be made available on request.

## References

- [1] H. Sung, et al., Global cancer statistics 2020: GLOBOCAN estimates of incidence and mortality worldwide for 36 cancers in 185 countries, *CA Cancer J. Clin.* 71 (3) (2021) 209–249.
- [2] C. Stewart, C. Ralyea, S. Lockwood, Ovarian cancer: an integrated review, *Semin. Oncol. Nurs.* 35 (2) (2019) 151–156.
- [3] C. Halbur, et al., siRNA-conjugated nanoparticles to treat ovarian cancer, *SLAS Technol.* 24 (2) (2019) 137–150.
- [4] K. Kariko, et al., Incorporation of pseudouridine into mRNA yields superior nonimmunogenic vector with increased translational capacity and biological stability, *Mol. Ther.* 16 (11) (2008) 1833–1840.
- [5] B.R. Anderson, et al., Nucleoside modifications in RNA limit activation of 2'-5'-oligoadenylate synthetase and increase resistance to cleavage by RNase L, *Nucleic Acids Res.* 39 (21) (2011) 9329–9338.
- [6] M. Sioud, G. Furset, L. Cekaite, Suppression of immunostimulatory siRNA-driven innate immune activation by 2'-modified RNAs, *Biochem. Biophys. Res. Commun.* 361 (1) (2007) 122–126.
- [7] B. Hu, et al., Therapeutic siRNA: state of the art, *Signal Transduct. Target. Ther.* 5 (1) (2020) 101.
- [8] D.M. Lynn, R. Langer, Degradable poly(b-amino esters): synthesis, characterization, and self-assembly with plasmid DNA, *J. Am. Chem. Soc.* 122 (2000) 10761–10768.
- [9] Y. Jin, et al., Spermine-based poly( $\beta$ -amino ester)s for siRNA delivery against mutated KRAS in lung cancer, *Mol. Pharm.* (2023).
- [10] A.P.E. Kromer, et al., Design of experiments grants mechanistic insights into the synthesis of spermine-containing PBAE copolymers, *ACS Appl. Mater. Interfaces* 16 (29) (2024) 37545–37554.
- [11] Y. Li, et al., Hyperbranched poly(beta-amino ester)s (HPAEs) structure optimisation for enhanced gene delivery: non-ideal termination elimination, *Nanomater. (Basel)* 12 (21) (2022).
- [12] C. Fornaguera, et al., Engineering oncogene-targeted anisamide-functionalized pBAE nanoparticles as efficient lung cancer antisense therapies, *RSC Adv.* 13 (43) (2023) 29986–30001.
- [13] A.G. Berger, et al., Poly(beta-aminoester) physicochemical properties govern the delivery of siRNA from electrostatically assembled coatings, *Biomacromolecules* (2024).
- [14] Y. Jin, et al., Role of hydrophobic modification in spermine-based poly(beta-amino ester)s for siRNA delivery and their spray-dried powders for inhalation and improved storage, *Biomacromolecules* 7 (2024) 4177–4191.
- [15] J.T. Müller, et al., Nebulization of RNA-loaded micelle-embedded polyplexes as a potential treatment of idiopathic pulmonary fibrosis, *ACS Appl. Mater. Interfaces* (2025).
- [16] I. Hellström, et al., Overexpression of HER-2 in ovarian carcinomas, *Cancer Res.* 61 (6) (2001) 2420–2423.
- [17] H.M. Shepard, Trastuzumab: dreams, desperation and hope, *Nat. Rev. Cancer* 24 (5) (2024) 287–288.
- [18] V.L. Cruz, et al., Binding affinity of trastuzumab and pertuzumab monoclonal antibodies to extracellular HER2 domain, *Int. J. Mol. Sci.* 24 (15) (2023).
- [19] J. Wu, The Enhanced permeability and retention (EPR) effect: the significance of the concept and methods to enhance its application, *J. Pers. Med.* 11 (8) (2021).
- [20] S. Carneiro, J.T. Müller, O.M. Merkel, Targeted molecular therapeutics for pulmonary diseases: addressing the need for precise drug delivery, *Handb. Exp. Pharmacol.* (2024).
- [21] M. Shan, et al., Distinguishing the cellular transport of folic acid conjugated nano-drugs among different cell lines by using force tracing technique, *Mol. Pharm.* (2023).
- [22] T. Rheinfrank, et al., Three is a magic number: tailored clickable chelators used to determine optimal RGD-peptide multiplicity in alphavbeta6-integrin targeted (177)Lu-labeled cancer theranostics, *Bioconjug. Chem.* (2024).
- [23] X. Zhu, et al., Inhalable dry powder prepared from folic acid-conjugated docetaxel liposomes alters pharmacodynamic and pharmacokinetic properties relevant to lung cancer chemotherapy, *Pulm. Pharmacol. Ther.* 55 (2019) 50–61.
- [24] National Center for Biotechnology Information. *PubChem Compound Summary for Trastuzumab*. [cited 20.01.2025; Available from: <https://pubchem.ncbi.nlm.nih.gov/compound/Trastuzumab>].
- [25] Hermanson, G.T., *Bioconjugates Techniques*. 1. Edition ed. 1996: Academic Press.
- [26] L. Lu, et al., Chemical conjugation strategies for the development of protein-based subunit nanovaccines, *Vaccines (Basel)* 9 (6) (2021).
- [27] D.C. Jurgens, et al., Tailoring lipid nanoparticles for T-cell targeting in allergic Asthma: insights into efficacy and specificity, *Eur. J. Pharm. Biopharm.* (2024) 114242.
- [28] M. Ripoll, et al., Supramolecular bioconjugation strategy for antibody-targeted delivery of siRNA, *Bioconjug. Chem.* (2024).
- [29] F. Eckerdt, J. Yuan, K. Strebhardt, Polo-like kinases and oncogenesis, *Oncogene* 24 (2) (2005) 267–276.
- [30] K. Strebhardt, A. Ullrich, Targeting polo-like kinase 1 for cancer therapy, *Nat. Rev. Cancer* 6 (4) (2006) 321–330.
- [31] Z. Wang, et al., Folate-mediated targeted PLK1 inhibition therapy for ovarian cancer: a comparative study of molecular inhibitors and siRNA therapeutics, *Acta Biomater.* 138 (2022) 443–452.
- [32] J. Wu, et al., Polo-like kinase 1 induces epithelial-to-mesenchymal transition and promotes epithelial cell motility by activating CRAF/ERK signaling, *Elife* 5 (2016).
- [33] M. Reda, et al., PLK1 and EGFR targeted nanoparticle as a radiation sensitizer for non-small cell lung cancer, *Cancer Lett.* 467 (2019) 9–18.
- [34] A.D. Judge, et al., Confirming the RNAi-mediated mechanism of action of siRNA-based cancer therapeutics in mice, *J. Clin. Invest.* 119 (3) (2009) 661–673.
- [35] X. Liu, R.L. Erikson, Polo-like kinase (Plk1) depletion induces apoptosis in cancer cells, *Proc. Natl. Acad. Sci. U. S. A.* 100 (10) (2003) 5789–5794.
- [36] G. Chhabra, et al., Role of PLK1/NUMB/NOTCH in epithelial-mesenchymal transition in human melanoma, *npj Precis. Oncol.* 8 (1) (2024) 6.
- [37] X. Ye, R.A. Weinberg, Epithelial-mesenchymal plasticity: a central regulator of cancer progression, *Trends Cell Biol.* 25 (11) (2015) 675–686.
- [38] M. Cherri, et al., Power of the disulfide bond: an ideal random copolymerization of biodegradable redox-responsive hyperbranched polyglycerols, *Biomacromolecules* 25 (1) (2024) 119–133.
- [39] R. Kandil, et al., Targeted GATA3 knockdown in activated T cells via pulmonary siRNA delivery as novel therapy for allergic asthma, *J. Control. Release* (2023).
- [40] Y. Xie, et al., Targeted delivery of siRNA to activated T cells via transferrin-polyethylenimine (Tf-PEI) as a potential therapy of asthma, *J. Control. Release* 229 (2016) 120–129.
- [41] R. Kandil, et al., Coming in and finding out: blending receptor-targeted delivery and efficient endosomal escape in a novel bio-responsive siRNA delivery system for gene knockdown in pulmonary T cells, *Adv. Ther. (Weinh)* 2 (7) (2019).
- [42] J. Schindelin, et al., Fiji: an open-source platform for biological-image analysis, *Nat. Methods* 9 (7) (2012) 676–682.
- [43] K.M. Steinegger, et al., Molecular dynamics simulations elucidate the molecular organization of poly(beta-amino ester) based polyplexes for siRNA delivery, *Nano Lett.* (2024).
- [44] N.J. Agard, et al., A comparative study of bioorthogonal reactions with azides, *ACS Chem. Biol.* 1 (10) (2006) 644–648.
- [45] H. Wiig, C.C. Gyenge, O. Tenstad, The interstitial distribution of macromolecules in rat tumours is influenced by the negatively charged matrix components, *J. Physiol.* 567 (Pt 2) (2005) 557–567.
- [46] T. Stylianopoulos, EPR-effect: utilizing size-dependent nanoparticle delivery to solid tumors, *Ther. Deliv.* 4 (4) (2013) 421–423.
- [47] R. Rampado, D. Peer, Design of experiments in the optimization of nanoparticle-based drug delivery systems, *J. Control. Release* 358 (2023) 398–419.
- [48] Y. Qin, et al., Evaluation of a DoE based approach for comprehensive modelling of the effect of lipid nanoparticle composition on nucleic acid delivery, *Biomaterials* 299 (2023) 122158.
- [49] A. Perna, et al., Different cell cycle modulation in SKOV-3 ovarian cancer cell line by anti-HIV drugs, *Oncol. Res.* 25 (9) (2017) 1617–1624.
- [50] Y. Wang, et al., Anticancer activity of sugiol against ovarian cancer cell line SKOV3 involves mitochondrial apoptosis, cell cycle arrest and blocking of the RAF/MEK/ERK signalling pathway, *Arch. Med. Sci.* 16 (2) (2020) 428–435.

- [51] Z. Wang, et al., HER-2-mediated nano-delivery of molecular targeted drug potently suppresses orthotopic epithelial ovarian cancer and metastasis, *Int. J. Pharm.* 625 (2022) 122126.
- [52] A. Langer, et al., A new spectral shift-based method to characterize molecular interactions, *Assay Drug Dev. Technol.* 20 (2) (2022) 83–94.
- [53] C. Mehner, et al., EGFR as a prognostic biomarker and therapeutic target in ovarian cancer: evaluation of patient cohort and literature review, *Genes Cancer* 8 (5–6) (2017) 589–599.
- [54] W. Yan, et al., Plk1 promotes the migration of human lung adenocarcinoma epithelial cells via STAT3 signaling, *Oncol. Lett.* 16 (5) (2018) 6801–6807.
- [55] L. Isert, et al., An in vitro approach to model EMT in breast cancer, *Int. J. Mol. Sci.* 24 (9) (2023).